

Climate-driven interannual ice mass evolution in Greenland

I. Bergmann^a, G. Ramillien^b, F. Frappart^b

^a*Helmholtz-Centre Potsdam, GFZ German Research Centre for Geosciences, Potsdam, Germany*

^b*Université de Toulouse, UPS, OMP, GET, Toulouse, France*

Abstract

We re-evaluate the Greenland mass balance for the recent period using low-pass Independent Component Analysis (ICA) post-processing of the Level-2 GRACE data (2002-2010) from different official providers (UTCSR, JPL, GFZ) and confirm the present important ice mass loss in the range of -70 and -90 Gt/y of this ice sheet, due to negative contributions of the glaciers on the east coast. We highlight the high interannual variability of mass variations of the Greenland Ice Sheet (GrIS), especially the recent deceleration of ice loss in 2009-2010, once seasonal cycles are robustly removed by Seasonal Trend Loess (STL) decomposition. Interannual variability leads to varying trend estimates depending on the considered time span. Correction of post-glacial rebound effects on ice mass trend estimates represents no more than 8 Gt/y over the whole ice sheet. We also investigate possible climatic causes that can explain these ice mass interannual variations, as strong correlations between GRACE-based mass balance and atmosphere/ocean parallels are established: (1) changes in snow accumulation, and (2) the influence of inputs of warm ocean water that periodically accelerate the calving of glaciers in coastal regions and, feed-back effects of coastal water cooling by fresh currents from glaciers melting. These results suggest that the Greenland mass balance is driven by coastal sea surface temperature at time scales shorter than accumulation.

Keywords: ice sheets, mass balance estimates, Greenland, GRACE

Email addresses: Inga.Bergmann@gfz-potsdam.de (I. Bergmann),
guillaume.ramillien@get.obs-mip.fr (G. Ramillien),
frederic.frappart@get.obs-mip.fr (F. Frappart)

1. Introduction

The mass balance of the Greenland Ice Sheet (GrIS), and its contribution to sea level rise, are of high interest in the context of global warming. According to the latest IPCC report (2007), melting of the whole GrIS would contribute nearly 7m to sea level rise. Even a less substantial mass loss would have a strong impact on sea level rise. Over the last twenty years, observations of the GrIS show an acceleration of ice mass loss caused by rapid glacier flow on the southeast and northwest coasts (see Allison et al. (2009) and Zwally et al. (2011) for reviews), in response to the recent warming affecting both the atmosphere (Box and Cohen, 2006) and sea water (Hanna et al., 2009). Nevertheless, analysis of changes in the glaciers reveals a succession of periods of mass loss acceleration and deceleration.

Since its launch in March 2002, the GRACE mission has demonstrated great potential for studying the ice sheet mass changes. The GRACE data have been increasingly used for assessing mass balance of Greenland and Antarctica. First studies revealed a significant mass loss of Greenland with an acceleration of melting starting in 2004 (Velicogna and Wahr, 2005, 2006; Chen et al., 2006; Luthcke et al., 2006; Ramillien et al., 2006). Mass loss occurred mainly on the east coast of Greenland whereas the interior of the continent exhibited a small mass increase (Luthcke et al., 2006; Wouters et al., 2008). Recent studies showed acceleration of the mass loss during 2006-2008 (Velicogna, 2009) and a deceleration during 2008-2009 (Chen et al., 2011). Nevertheless, the results obtained so far are highly dependent on the length of the GRACE time series, the chosen data set, the nature of the post-processing, and the method for computing linear trends (i.e., with or without adjusting the seasonal components). Results can vary by a factor ~ 3 depending on the data set (e.g. CSR, GFZ or JPL; Baur et al., 2009). From these previous GrIS mass balance estimates, linear trends were simply computed over the complete (or parts of the) period of availability of the GRACE data, assuming the ice melting to be constant in time. Only Velicogna (2009) and Rignot et al. (2011) estimated accelerations for 2004 and 2008-2009.

In this study, we re-evaluate the Greenland mass balance over a longer time span (October 2002 - July 2010), using Level-2 GRACE data from the Science Data Centre

31 (UTCSR, GFZ and JPL) and different post-processing techniques (Gaussian and Inde-
32 pendent Component Analysis-based approaches) at continental and ice field scales. We
33 also analyze the interannual variability of the mass balance using the robust Seasonal
34 Trend Decomposition by Loess (LOcally wEighted Scatterplot Smoothing) (STL) ap-
35 proach. The non-stationarity of the mass balance is then related to climate forcings
36 from the atmosphere and the ocean through comparisons with snow depths (SD) and
37 sea surface temperatures (SST).

38 **2. Data sets**

39 *2.1. GRACE-based water mass variations*

40 Since its launch in March 2002, the Gravity Recovery And Climate Experiment
41 (GRACE) mission, consisting of a pair of co-orbiting satellites at an altitude of 400-
42 450 km, provides a systematic mapping of the spatio-temporal variations of the Earth's
43 gravity field. These are estimated with an unprecedented precision of ~ 1 cm in terms of
44 geoid height (Tapley et al., 2004), or equivalently ~ 15 -20 cm in equivalent-water thick-
45 ness when averaged in regions of 300x300 of square kilometers (Ramillien et al., 2008;
46 Schmidt et al., 2008). The Level-2 GRACE solutions consist of monthly Stokes coeffi-
47 cients (i.e., normalized spherical harmonics of the geo-potential) estimated by a least-
48 squares adjustment of GRACE orbit measurements -especially very accurate inter-
49 satellite K-Band Range (KBR) variations- made by different official providers [Ge-
50 oForschungsZentrum (GFZ) in Potsdam Germany, Center of Space Research at Uni-
51 versity of Texas (UTCSR) in Austin, TX, Jet Propulsion Laboratory (JPL) in Pasadena,
52 CA]. In this process, the Stokes coefficients are corrected for known atmospheric and
53 oceanic gravitational contributions (Bettadpur, 2007), so that the residuals represent
54 non-modeled phenomena, mainly variations in land water storage, glaciers, and ice
55 sheet mass. These Level-2 GRACE solutions are available at: <ftp://podaac.jpl.nasa.gov/grace/>
56 up to harmonic degree of 50-60 (i.e., spatial resolution of 333-400 km), and the corre-
57 sponding global $1^\circ \times 1^\circ$ grids of equivalent-water heights are also downloadable. In our
58 study, we use monthly GFZ, UTCSR and JPL solutions from 04/2002 to 07/2010.
59 The GRACE solutions suffer from the presence of an unrealistic high-frequency noise

60 appearing as north-south striping, caused by orbit resonance during the Stokes coeffi-
61 cient determination and aliasing with short-term oceanic and atmospheric phenomena
62 that are not well modeled. Several post-processing methods, such as low-pass Gaussian
63 filtering, have been proposed to solve this problem (Jekeli, 1981; Swenson and Wahr,
64 2002). However most of them suffer from the risk of losing signal energy in the spec-
65 trum truncation (i.e., drastic loss of spatial resolution). This also needs arbitrary tuning
66 of required parameters (e.g., a priori level of noise, cutting spatial frequencies,...) in
67 absence of criteria. To get rid of the noise in the L-2 GRACE solutions, we preferred to
68 use the global ICA estimates obtained by combination of GFZ/UTCSR/JPL solutions,
69 to isolate statistically independent components of the observed gravity field, in particu-
70 lar the continental water storage contribution that we compared with continental water
71 storage estimated from classical Gaussian-filtered solutions.

72 2.2. ICA solutions

73 A post-processing method based on ICA (Comon, 1994; De Lathauwer et al.,
74 2000) was applied to the Level-2 GRACE solutions prefiltered with Gaussian filters of
75 400 km and 500 km of radius. This so-called blind source separation (BSS) approach
76 does not require a priori information, except the assumption of statistical independence
77 of the elementary sources that compose the total measured signals. Taking into account
78 the consideration that the GRACE Level-2 products from CSR, GFZ and JPL are dif-
79 ferent observations of the same monthly gravity anomaly, and that the land hydrology
80 and the north-south stripes are the independent sources.

81 Assuming that the observations y collected from N sensors are the combination of P
82 ($N \geq P$) independent sources represented by the source vector x , they can be written
83 as a linear statistical model:

$$y = Mx, \quad (1)$$

84 where M is the mixing matrix whose elements m_{ij} ($1 \leq i \leq N$, $1 \leq j \leq P$) in-
85 dicate to what extent the j th source contributes to the i th observation. The columns
86 $\{m_j\}$ are the mixing vectors. ICA aims at estimating the mixing matrix M and/or the
87 corresponding realizations of the source vector x , only knowing the realizations of the

88 observation vector y , under the following assumptions: i) the mixing vectors are lin-
89 early independent, and ii) the sources are statistically independent. The contributors to
90 the observed gravity field are forced to be uncorrelated, numerically only considering
91 completely objective constraints. The efficiency of ICA to separate gravity signals and
92 noise from combined GRACE solutions has previously been demonstrated on Level-2
93 solutions over land (Frappart et al., 2010, 2011). Series of ICA-estimated global maps
94 of continental and ice caps mass changes, computed over 08/2002-07/2010, are used
95 in this study to estimate the mass balance of Greenland.

96 2.3. *ECMWF Snow depth data*

97 We used the daily snow depth grids from the European Centre for Medium-Range
98 Weather Forecasts (ECMWF) ERA-interim reanalysis with a horizontal resolution of
99 $1.5^{\circ} \times 1.5^{\circ}$ (http://data-portal.ecmwf.int/data/d/interim_daily/; Dee et al. , 2011). These
100 grids were estimated from the improved snow scheme of the Hydrology Tiled ECMWF
101 Scheme of Surface Exchanges over Land (HTESSEL) land surface model. It includes a
102 new parametrization of snow density, incorporating a liquid water reservoir, and revised
103 formulations for the sub grid snow cover fraction and snow albedo (Dutra et al., 2010).
104 The daily grids of snow depth were averaged monthly over the period April 2002 to
105 July 2010, for comparisons with the total water storage derived from GRACE.

106 2.4. *NOAA Sea Surface Temperature*

107 In this study, we used the National Oceanic and Atmospheric Administration (NOAA)
108 Optimum Interpolation Sea Surface Temperature Analysis Version 2, available at
109 <http://www.esrl.noaa.gov/psd/>. They consist of weekly grids produced by optimal in-
110 terpolation (Reynolds and Smith, 1994). Monthly solutions are then estimated by lin-
111 ear interpolation of weekly fields to daily fields, and averaging the daily values over
112 a month. The monthly fields have a resolution of $1^{\circ} \times 1^{\circ}$ on a global half degree grid.
113 Data from April 2002 to July 2010 are used in this study.

114 3. Methodology

115 3.1. Mass anomalies from GRACE data

116 The monthly Stokes coefficients of the GRACE solutions are used to estimate mass
117 anomalies by spherical harmonic expansion (Wahr et al., 1998). After removing a tem-
118 poral average, monthly maps of surface mass density anomalies ($\Delta\sigma$) can be computed
119 as:

$$\Delta\sigma(\phi, \lambda, t) = \frac{a_e \rho_e}{3\rho_w} \sum_{l=2}^{\infty} \sum_{m=0}^l \frac{2l+1}{1+k_l} P_{lm}(\sin \phi) (\Delta C_{lm} \cos m\lambda + \Delta S_{lm} \sin m\lambda) \quad (2)$$

120 where a_e is the semi major axis, ρ_e the average density of the earth (5517 kg/m³),
121 ρ_w the density of water (1000 kg/m³), k_l are the elastic Love numbers of degree l ,
122 P_{lm} are the normalized associated Legendre Polynomials of degree l and order m , ϕ is
123 the geographical latitude, λ the geographical longitude, t the time and (ΔC_{lm} , ΔS_{lm})
124 are the fully normalized dimensionless spherical harmonic (Stokes) coefficients given
125 by GRACE. The $\Delta\sigma$ are given in meters of equivalent water height. The spherical
126 harmonic expansion has been performed up to degree and order 60 which leads to a
127 spatial grid resolution of ~ 333 km.

128 To remove the noise due to aliasing of short-term phenomena (inducing north-south
129 stripes) the solutions have to be filtered. In this work a Gaussian filter with a half width
130 radius of 400km and 500km was used. As mentioned in section 2.2, the Gaussian
131 filtered solutions are further destriped by applying of the ICA method.

132 Mass variations $\Delta\sigma$ are computed at each time step and grid point, and have been
133 further averaged in the boundaries of the GrIS and subregions.

134 3.2. Correction of the Post-Glacial Rebound

135 Over Canada and northwestern Europe, the last deglaciations (~ 20 k-years ago)
136 of thick ice sheets caused rapid deloadings of ice mass. Because of its viscoelastic
137 behavior, i.e. Post Glacial Rebound (PGR), the Earth's mantle is still continuing a
138 non negligible isostatic re-adjustment (Peltier, 2004). As a consequence of this long-
139 term deformation, the Earth's surface and gravity field are still affected by PGR at

140 linear rates. For example, in the South of Hudson Bay in Canada, the uplift of the
 141 surface measured at GPS sites reaches 1.1 cm/yr (Sella et al., 2007). Knowledge of the
 142 deglaciation history and the Earth's mantle viscosity remains limited to uncertainties
 143 in PGR modeling. However, according to independent models, PGR geographically-
 144 averaged over Greenland shows negative trends weaker than 10 Gt/yr, and is considered
 145 by some authors to be weak compared to ice mass loss. Using different PGR models,
 146 comparable PGR estimates, from 7 or 8 Gt/yr were found (Velicogna and Wahr, 2006;
 147 Velicogna, 2009) considering the ICE-5G model of Peltier (2004), and up to 9 Gt/y
 148 (Ramillien et al., 2006) using the IJ-2005 model developed by Ivins and James (2005).
 149 As it is available at the GRACE Tellus website (<http://grace.jpl.nasa.gov/data/pgr>), we
 150 consider the Paulson et al. (2007) model based on the ICE-5G ice model and a tuning of
 151 mantle viscosity contrasts and crust thickness. The $1^\circ \times 1^\circ$ grid of PGR trend has been
 152 downloaded from this website, and the Stokes coefficients of the PGR have been con-
 153 verted into rates of surface mass change and expressed in mm of water height per year.
 154 Degree-one terms were omitted as they are not included in the GRACE solutions. The
 155 results were smoothed using a Gaussian averaging function of 400 and 500 km radius.
 156 Over the whole of Greenland, we found a PGR trend close to -8 Gt/yr, representing -4
 157 mm/yr of equivalent-water height. For each time step the modeled PGR contribution
 158 has been removed from the filtered GRACE mass anomalies.

159 When interpreting the PGR-corrected Greenland mass balance, we keep in mind that
 160 the PGR model uncertainty can represent an important source of error.

161 3.3. *Seasonal-Trend Decomposition by Loess (STL) Method*

162 The STL method, based on locally weighted regression (Cleveland et al., 1990),
 163 is a robust and computationally efficient approach commonly used to decompose time
 164 series into trend (T_v), seasonal (S_v), and residual (R_v) components:

$$Y_v = T_v + S_v + R_v \quad (3)$$

165 STL is an iterative method consisting of two recursive procedures, one nested within
 166 the other, called the inner and the outer loops. The trend and seasonal estimates are

167 progressively refined in the inner loop in each iteration. After one complete run of the
 168 inner loop, robustness weights are computed in the outer loop. These weights are used
 169 in the next run of the inner loop to reduce the influence of outliers in the trend and
 170 seasonal signal. The local weights ϑ_v of the values depend on the time steps to the
 171 observed time in a chosen window with size q . A polynomial with power d is fitted to
 172 the weighted data.

173 The inner loop contains six steps. In the first step of the k th run of the inner loop, the
 174 time series Y_v is detrended with T_v^k :

$$Y_v^{detrend} = Y_v - T_v^k. \quad (4)$$

175 Then, every sub-cycle time series is smoothed by locally weighted regression and the
 176 results are stored in C_v^{k+1} (step 2). In the third step the smoothed sub-cycle time
 177 series are processed using a low pass filter. The low pass filter is composed of three
 178 consecutive averaging means, followed by a locally weighted regression. The low
 179 pass filtered values are stored in L_v^{k+1} . The estimated low pass filtered values of the
 180 seasonal sub-cycles are then removed from the smoothed sub-cycle time series of step
 181 2 to receive the seasonal signal S_v^{k+1} (step 4):

$$S_v^{k+1} = C_v^{k+1} - L_v^{k+1}. \quad (5)$$

182 In the next step (step 5), the original time series is reduced by the seasonal signal:

$$Y_v^{deseason} = Y_v - S_v^{k+1}. \quad (6)$$

183 In the last step (step 6) the reduced time serie from step 5 is smoothed by locally
 184 weighted regression with $d = 1$ to receive the updated trend signal T_v^{k+1} .

185 In the outer loop the trend and seasonal signal are used for computing the remaining
 186 signal R_v :

$$R_v = Y_v - T_v^{k+1} - S_v^{k+1}. \quad (7)$$

187 For each time step a robustness weight ρ_v is determined. Outliers will have a very small
188 or zero weight. In the next run of the inner loop the robust weight will be multiplied to
189 the weights ϑ_v in the locally weighted regression in step 2 and 6.

190 The Fortran-Code for the STL-Method has been provided at the following webpage:
191 <http://www.stat.purdue.edu/wsc/localfitsoft.html>. For an easy start into the method the
192 function `stleze.f` has been used. In this function just the main necessary parameters
193 have to be entered by the user:

194 1) The number of observations n_p which are included in each period. We have time
195 series with monthly resolution and an annual signal, choosing $n_p = 12$.

196 2) The number of iterations of the inner (n_i) and outer (n_o) loop. Because, that the
197 convergence of estimating the different components of the signal is very fast, n_i can
198 be set to 1. If a robust estimation of the signals is preferred, the determination of the
199 robust weight in the outer loop is done until the convergence criteria is reached, or with
200 a maximum of $n_o = 15$.

201 3) In step 2 the estimated seasonal signal is smoothed by Loess with the parameters
202 $d = 1$ and $q = n_s$. The seasonal signal becomes smoother with increasing n_s . At
203 minimum, n_s has to be odd and greater than 6. Due to this fact $n_s = 7$ has been chosen.

204 4) In step 3 the smoothing with Loess, with parameter $d = 1$ and $q = n_l$, is applied. The
205 weight factor n_l has to be chosen as the least odd number equal to n_p . In this case
206 with $n_p = 12$, then $n_l = 13$.

207 5) In the last step (step 6), the trend signal is smoothed with Loess with $d = 1$ and
208 $q = n_t$. The parameter n_t should be the least odd integer value greater or equal to

$$n_t \geq \frac{1.5 * n_p}{1 - \frac{1.5}{n_s}} \quad (8)$$

209 With the above given values for the parameters n_p and n_s , then $n_t = 21$.

210 4. Results and Discussion

211 4.1. Re-evaluation of the recent Greenland mass change

212 Gaussian-filtered and smoothed ICA solutions were averaged over Greenland by
213 simply using a geographical mask over the period 2002-2010. Figure 1 presents the six

214 mean ice fields composing the Greenland ice sheet (acc. to Luthcke et al., 2006). The
215 corresponding ICA-based time series were corrected for the seasonal signal by apply-
216 ing the STL decomposition (explained in paragraph 3.3). Velicogna (2009) proposed
217 an additional filtering to cancel the long term and periodic contributions in the GRACE
218 data, based on the least-square adjustment of annual, semi-annual, trend and constant
219 terms using 13-month running windows. Instead of fitting empirical periodic varia-
220 tions, we preferred to apply the more robust STL method for extracting the long-term
221 signals. To illustrate the benefit of using the STL decomposition, Fig. 2 compares the
222 Greenland mass balance based on the method developed here (STL, ICA), to classical
223 Gaussian filtering. The decreasing behavior of these curves confirms the mass deple-
224 tion of this ice sheet due to important melting during the GRACE period. Moreover,
225 these GRACE-derived time series also contain annual and sub-annual signals that need
226 to be isolated in order to extract the interannual ice mass variations. Differences be-
227 tween ICA and Gaussian filtered estimates are not always correlated for wavelengths
228 less than 1 year, and they can reach 100 mm of equivalent-water height. These short-
229 term differences can be accounted for a reduction of the residual noise by ICA after the
230 Gaussian low-pass filtering. Fig. 2b presents the STL-smoothed time series containing
231 the interannual variations of GrIS ice mass, which are not a simple straight line, sug-
232 gesting that GrIS ice mass loss cannot be represented by a constant slope. In the next
233 sections, we attempt to explain the presence of such interannual variations by estab-
234 lishing correlations in time with climate forcings.

235 Depending on the chosen period and time length, the linear trends computed along
236 the time series are not constant. For example, there are obvious accelerations of ice
237 melting (Velicogna and Wahr, 2006; Velicogna, 2009), and a relative deceleration in
238 2009-2010, in agreement with the results found by Rignot et al. (2011) for Greenland
239 during the last years. The change of the GrIS mass balance for the complete GRACE
240 period (i.e., between 2003 and 2010) still exhibits a huge mass loss, even before the
241 constant negative rate of ~ -8 Gt/yr for PGR is removed from the linear trend estimates.
242 The amplitude of these trend estimates clearly varies with the GRACE solution provider
243 (i.e., CSR, GFZ, JPL) and the post-processing (i.e., ICA or only Gaussian low-pass fil-
244 tering). In terms of sensitivity relative to the GRACE solution source, the lowest values

245 are systematically obtained with the JPL solutions. This is probably due to some spe-
246 cific pre-processings of the GRACE measurements made by this provider. Low linear
247 trends were already found by Baur et al. (2009) using JPL solutions over Greenland
248 while CSR solutions give values twice as large (see Table 1).

249 Use of ICA instead of Gaussian filtering makes the GrIS ice mass time series smoother.
250 As a consequence ICA-based linear trends are smaller. In the case of Gaussian low-pass
251 filtering, the larger the cutting wavelength the lower the trend estimate. By using the
252 400-km Gaussian-filtered solutions, the 2003-2010 rate ranges from -35 ± 2 Gt/yr for
253 JPL to -89 ± 2 Gt/yr for CSR. With the 500-km ICA solutions, this rate varies from -56
254 ± 2 Gt/yr for JPL to -74 ± 3 Gt/yr for CSR. Whatever type of post-processing is used,
255 using the JPL solutions yields to the lowest linear trend estimates, with magnitudes
256 <60 Gt/yr for ICA processing, and <40 Gt/yr for the Gaussian filter, once correcting
257 from the PGR effects.

258 Comparison with PGR-corrected GrIS ice mass loss estimates from previous studies
259 leads to important differences (see Table 1 and Figure 3). These differences can be
260 explained by the different time spans considered in this study and the high interan-
261 nual variability of the GrIS ice mass change, as previously shown on the Fig.2a-b. We
262 checked this by computing trends over different time spans. As shown in Figure 3,
263 trend estimates are highly dependent on both the considered time span and the method-
264 ology used. For instance, we obtained STL-base (and linear) trends of respectively
265 -96.5 (-100.3), -78.3 (-74.7), -106.8 (-115.2) Gt/yr for the periods 04/2002-11/2009,
266 04/2002-03/2005, 04/2005-11/2009, using CSR solutions Gaussian filtered with a ra-
267 dius of 400 km, whereas Chen et al. (2011) found linear trends of respectively -219 ,
268 -144 , -248 Gt/yr over the same time periods using CSR solutions, after low-pass Gaus-
269 sian filtering using a radius of 300 km and correcting of leakage and biases of GRACE.
270 Our trend estimates using Gaussian-filtered solutions are slightly lower (i.e., around
271 -80 Gt/yr), but remain consistent in amplitude with the results of previous works (e.g.,
272 Ramillien et al. (2006) obtained -109 Gt/yr considering the period 07/2003 - 03/2005).
273 The Gaussian filter-based estimates often differ by more than a factor 2, since Wouters
274 et al. (2008) found -171 Gt/yr for the period 03/2003 -01/2008, Baur et al. (2009) ob-
275 tained -222 ± 13 , -178 ± 22 , -88 ± 21 Gt/yr for the period 08/2002-07/2008 considering

276 the CSR, GFZ, and JPL solutions, and Chen et al. (2011) proposed a value of -219
277 Gt/yr for 04/2002-11/2009. Velicogna and Wahr (2006) found an extreme value of -
278 240 Gt/yr considering a shorter period. In fact, these latter authors proposed to multiply
279 artificially their GrIS ice mass estimate by a scaling factor of ~ 2 , to compensate the
280 leakage effects over Greenland (i.e., loss of signal energy due to the spherical harmon-
281 ics truncation at degree 50-60). The large value of this scaling factor over Greenland
282 was empirically estimated from global hydrology model simulations (see Velicogna
283 and Wahr (2006), p.331). It explains mostly the difference of previous studies and
284 our Gaussian filter-based estimates. The lowest estimates are found by using the ICA-
285 based time series (< 70 Gt/y). ICA reduces the magnitude of the North-South stripes
286 that are not correlated with continental hydrology signals (Frappart et al., 2010, 2011).
287 The choice of the cutting wavelength before ICA separation has strong consequences
288 on the level of noise in the pre-filtered solutions, and thus on the amplitude of the lin-
289 ear trend estimates. When the noise in the pre-filtered solutions increases, the standard
290 deviations of the linear trend estimates do the same. In other words, a large amount
291 of error in the trend estimate may come from the dispersion of the starting points on
292 which a straight line is fitted.

293 Consequently, the noise-free ICA-based solution corresponds to a sea level contribu-
294 tion of 0.19 mm/yr. This is less than the one proposed by previous studies, in particular
295 by Velicogna and Wahr (2006) (0.5 ± 0.1 mm/yr) for the same period 2002 - 2006. The
296 most important point is that this GrIS contribution varies from year to year and thus
297 cannot be simply represented by a constant trend. One may wonder if adjusting a trend
298 on time series of mass variation makes physical sense for such short time spans (i.e., a
299 few years). Instead of considering a constant rate of ice mass loss, we propose integrat-
300 ing numerically the total ice mass variations versus time, to establish a more realistic
301 mass balance of the melting GrIS, which remains completely time-dependent at the
302 multi-year time scale.

303 Figure 4 shows trend maps of the GrIS estimated from the Gaussian and STL filtered
304 solutions for two different time spans. It can be shown that the linearly adjusted trends
305 also depend geographically upon the chosen time span. Considering a short period
306 (2003-2007) makes small positive trends appear in the north east of Greenland, whereas

307 considering the complete time span (2003-2010) does not reveal any positive anomalies.
308 For the period 2003-2007, the northern patterns of the STL-decomposed mass
309 trend remain consistent with the ones described by Zwally et al. (2011) using ICESat
310 data.

311 4.2. Regional mass balances

312 Time series of the mass balance for different Greenland ice-field basins were computed
313 using the geographical boundaries from Luthcke et al. (2006). They are presented on Fig. 5.
314 If the whole GrIS exhibits a clear mass depletion over 2003-2010, the situation is more
315 contrasted at regional scale. The highest mass loss occurs in the southeastern part of the
316 continent with an average rate of -107 Gt/yr and -120 Gt/yr for ICA and Gaussian solutions
317 respectively (Fig. 3c, d, e). In general, mass depletion is larger in coastal regions than
318 inside the continent due to a huge amount of ice lost by coastal glaciers along the south
319 coast.

320 Our regional estimates remain numerically comparable to the per-basin mascons values
321 found by Luthcke et al. (2006) for the period 2003-2005, where the most significant mass
322 loss occurs in the southeastern regions of Greenland (i.e., -71 Gt/yr). Once again, the
323 difference with our estimates comes from the facts that: (i) the period of time we consider
324 is longer (e.g., non-stationarity of the signals at inter-annual time-scales), and (ii)
325 mascons solutions probably provides a smoother solution as it is based on spatial a priori
326 constraints of a few hundreds of km (Rowlands et al., 2005).

327 4.3. Comparison with simulated snow depth

328 To explain the interannual variations of the GrIS, comparisons between GRACE-derived
329 mass changes and simulated snow depth (SD) were achieved. Assuming that the horizontal
330 displacements are low at the top of the ice fields (and then accelerate progressively down to
331 the coast), and assuming that the mass balance depends only upon vertical mass fluxes (i.e.
332 snow fall), we first computed correlation maps between the monthly mass anomalies from
333 the different GRACE products and the monthly SD from ERA-interim over the period 2003-
334 2010 (Fig. 6). The results for CSR (ICA 400 km), CSR (GAUSS 400 km), GFZ (GAUSS
335 400 km), and JPL (GAUSS 400 km) are

336 presented on Fig. 6a, b, c, and d respectively. We chose to only present the correlation
337 map for that ICA CSR solution as the results obtained using GFZ and JPL solutions
338 are very similar by construction (Frappart et al., 2010). High correlation coefficients
339 (>0.7) are obtained over northern Greenland for the ICA, and CSR and GFZ Gaussian
340 solutions, except in the northeastern part where ICA products exhibit negative corre-
341 lation with snow depth. On the contrary, for the JPL Gaussian-filtered solutions high
342 correlations are present only on the northwestern part of Greenland. For the southern
343 part, CSR and JPL Gaussian solutions present medium to high correlation coefficients
344 in the west, and negative correlations in the east, whereas GFZ Gaussian solutions ex-
345 hibit negative correlations except over a small region in the center where correlations
346 are low (0.3 to 0.4).

347 The spatial pattern of the correlation between SD and for GRACE solutions is more
348 consistent with other independent data sets for the ICA solutions. For these solutions,
349 the greater correlations are found on the higher altitudes (>2000 or 2500 m) where the
350 GrIS is nearly in balance due to small annual cycles and seasonal variations (Luthcke
351 et al., 2006), and negative correlations are found at lower elevations where precip-
352 itation is increasingly rainfall rather than snowfall due to a rise of air temperatures
353 (Krabill et al., 2000; Chylek et al., 2004; van den Broeke et al., 2009). In contrast,
354 negative correlations are present mainly on the southwest coast, in the southeast, and
355 in a small region in the northeast of Greenland. The time variations of the GrIS mass
356 anomalies in these regions show that the mass decreases (2003-2008) or is balanced
357 (2008-2010), even when snow depth increases (see basin 3 to 5 in Fig. 7). These
358 regions are covered with large glaciers, such as the Jacobshavn, Kangerlugssuaq and
359 Helheim glaciers. The latter two have experienced an acceleration of their depletion
360 rate in the recent years: acceleration in 2002-2003, deceleration in 2006, and accel-
361 eration in 2007 (Howat et al., 2007; Rignot et al., 2008). This spatial pattern is also
362 in good accordance with modeled mass changes and discharge of the GrIS over 2003-
363 2008 (van den Broeke et al., 2009), the anomalies of mean annual runoff (Hanna et al.,
364 2005), air temperatures (Hanna et al., 2008), and melting days (Mote, 2007; Tedesco
365 et al., 2011) during recent years: high correlations between SD and ICA solutions can
366 be related to increasing mass, negative anomalies of temperatures and melting days,

367 and vice versa. This result confirms that the mass balance of the GrIS is dominated
368 by snowfall in regions of high elevation and by glacier discharge in regions of lower
369 elevations.

370 4.4. Comparison with Sea Surface Temperature

371 The recently observed reduction of both extent and duration of winter sea-ice should
372 cause an increase of snowmelt and glacier discharge due to an advection of warmer
373 water from the ocean (Hanna et al., 2008). These observations coincide with a rapid
374 succession of retreats and advances of the largest outlet glaciers (Luckman et al., 2006;
375 Howat et al., 2007; Joughin et al., 2008; Moon and Joughin, 2008; Rignot et al., 2008)
376 and suggest that Sea Surface Temperature (SST) and deeper ocean temperatures may
377 have a strong impact on glacier dynamics (Hanna et al., 2009), especially when no
378 strong correlation between air temperature and glacier dynamics was observed (Mur-
379 ray et al., 2010).

380 We focus here on the largest glaciers, present in the south east of Greenland, in the
381 region where snow depth change is not correlated with the mass change observations
382 from GRACE (see Fig. 6 and basin 4 in Fig. 7). The mass variations derived from
383 GRACE in this region were compared with SST along the south east coast of Green-
384 land. Interannual trends of mass anomalies from GRACE and SST from NOAA are
385 presented on Fig. 8 for several glaciers (further abbreviated with G1-G4, see Fig. 1)
386 and locations in the Arctic Ocean (abbreviated with S1-S3). The interannual trends for
387 south east Greenland present a decrease of the mass loss starting in 2006, consistent
388 with the slow down and advance post-2005 of the glaciers' outlets, observed using mul-
389 tispectral and Synthetic Aperture Radar (SAR) images (Howat et al., 2008; Moon and
390 Joughin, 2008; Murray et al., 2010). The mass loss over the 2003-2010 time period
391 is larger for southern glaciers (-72 ± 1 mm/yr and -73 ± 2 mm/yr on average for ICA
392 and Gaussian solutions respectively at point G4) than for northern ones (-41 ± 1 mm/yr
393 and -44 ± 1 mm/yr in average for ICA and Gaussian solutions respectively at point G1).
394 These results are in good agreement with estimates of surface mass balance models,
395 which show that the largest variations of winter accumulation and runoff are located in
396 the southeastern parts of Greenland (Murray et al., 2010).

397 Comparisons of interannual mass changes and SST in the north show that an increase
398 (respectively a decrease) of SST is followed by an acceleration (respectively a decel-
399 eration) of the mass change, whereas a decrease (respectively an increase) of SST in
400 the south is followed by a deceleration (respectively an acceleration) of mass change.
401 Larger correlations are found for northern ocean points. It seems that glacier mass vari-
402 ations are strongly influenced by seasonal northern SST changes (succession of posi-
403 tive and negative temperature events) with a time lag of 120 to 240 days and impact
404 the SST in the south of Greenland, close to Fram Strait. This suggests that warm-
405 ing/cooling phases of coastal oceanic currents can cause dynamic glacier change, as a
406 negative feedback between glaciers and the East Greenland Coastal Current (EGCC)
407 evoked by Murray et al. (2010).

408 **5. Conclusion**

409 Our study presents a re-evaluation of the mass balance of the Greenland ice sheet
410 using the Level-2 GRACE solutions over the period October 2002-July 2010 and using
411 two post-processing methods to reduce noise and estimate trends. If our results corrob-
412 orate what was found previously for shorter time spans, the most recent observations
413 show, for the very first time since the launch of the GRACE mission, a decrease in mass
414 loss of the GrIS for all the considered sources (UTCSR, GFZ, and JPL) and several fil-
415 tering methods (Gaussian and Gaussian + ICA for averaging radii of 300, 400, and
416 500 km). The methodology, based on the combination of a Gaussian filter and an ICA
417 approaches, reduces contamination by the spurious north-south stripes, and provides
418 mass change rates more consistent with each other than classical filtering techniques.
419 The decrease of GrIS ice mass is clearly not constant in time, but contains interannual
420 variability suggesting that the ice mass melting is a transitional complex phenomenon.
421 In terms of methodology, we therefore remain very critical about simply fitting a sim-
422 ple straight line to a set of points that contains different levels of noise. There are
423 important implications in understanding the causes of an observed continuous sea level
424 change. If the mass contribution of the ice sheets melting to sea level is not constant
425 at interannual time scales, and less than previously expected, this means a larger steric

426 (i.e., thermal) contribution in response of global warming. We also attempted to inves-
427 tigate these long-term variations by studying correlations with climate variables. The
428 GrIS mass balance is governed inside the continent by the snow accumulation and by
429 the dynamics of glaciers in the coastal regions. The increase in snowfall since win-
430 ter 2008-2009 in the south and since 2009-2010 in the north, and also a deceleration
431 of the glacier discharge since 2008 reported in several studies using independent data,
432 are responsible for the decrease in mass loss of Greenland. The mass changes of the
433 glaciers present in the southwest of Greenland were found to be anticorrelated with the
434 SST of the Denmark strait. This confirms the assumption of Murray et al. (2010) that
435 glacier dynamics of southeast Greenland are controlled by the oceanic currents. Unfor-
436 tunately, the spatial resolution of the GRACE data (~ 333 km for harmonic coefficients
437 expanded up to degree 60) is insufficient to resolve fjord scales.

438 *Acknowledgements.* This work was done by I. Bergmann during a three-month internship at
439 CNES/GRGS, Observatoire Midi-Pyrénées, Toulouse, France in 2010. The authors wish to thank
440 Lucia Seoane (GET, OMP) for preprocessing the available years of GRACE and Pascal Gegout
441 (GET, OMP) for helping us with the processing of the ECMWF data, as well as A. Cazenave
442 (LEGOS, OMP) for fruitful discussions.

443 Allison, I., Alley, R.B., Fricker, H.A., Thomas, R.H., Warner, R., 2009. Ice sheet mass balance
444 and sea level. *Antarct. Sci.* 21, 413–426.

445 Baur, O., Kuhn, M., Featherstone, W.E., 2009. GRACE-derived ice-mass variations over Green-
446 land by accounting for leakage effects. *J. Geophys. Res.* Vol. 114, B06407.

447 Bettadpur, S., 2007. GRACE 327-734 (CSR-GR-03-01) Gravity Recovery and Climate Exper-
448 iment Level-2 Gravity Field Product User Handbook. Technical Report. Center for Space
449 Research, The University of Texas in Austin.

450 Box, J.E., Cohen, A.E., 2006. Upper-air temperatures around Greenland: 1964-2005. *Geophys.*
451 *Res. Lett.* 33, L12706.

452 van den Broeke, M., Smeets, P., Ettema, J., 2009. Surface layer climate and turbulent exchange
453 in the ablation zone of the west Greenland ice sheet. *Int. J. Climatol.* Vol. 29, p. 2309–2323.

454 Chen, J. L., Wilson, C. R., Tapley, B. D., 2006. Satellite gravity measurements confirm acceler-
455 ated melting of Greenland ice sheet. *Science* Vol. 313, 1958-1960.

- 456 Chen, J. L., Wilson, C. R., Tapley, B. D., 2011. Interannual variability of Greenland ice losses
457 from satellite gravimetry. *J. Geophys. Res.* 116, B07406.
- 458 Chylek, P., Box, J.E., Lesins, G., 2004. Global warming and the Greenland ice sheet. *Climatic*
459 *Change* Vol. 63, p. 201–221.
- 460 Cleveland, Robert, B., Cleveland, W.S., McRae, J.E., Terpenning, I., 1990. Stl: A seasonal-trend
461 decomposition procedure based on loess. *Journal of Official Statistics* Vol. 6, No. 1, p. 3–33.
- 462 Comon, P., 1994. Independent Component Analysis, A new concept. *Signal Process.* Vol. 36,
463 287-314.
- 464 De Lathauwer, L., De Moor, B., Vandewalle, J., 2000. An introduction to independent compo-
465 nent analysis. *J. Chemometr.* Vol. 14, 123-149.
- 466 Dee, D. P., Uppala, S. M., Simmons, A. J., Berrisford, P., Poli, P., Kobayashi, S., Andrae, U.,
467 Balmaseda, M. A., Balsamo, G., Bauer, P., Bechtold, P., Beljaars, A. C. M., van de Berg, L.,
468 Bidlot, J., Bormann, N., Delsol, C., Dragani, R., Fuentes, M., Geer, A. J., Haimberger, L.,
469 Healy, S. B., Hersbach, H., Hólm, E. V., Isaksen, L., Kållberg, P., Köhler, M., Matricardi, M.,
470 McNally, A. P., Monge-Sanz, B. M., Morcrette, J.-J., Park, B.-K., Peubey, C., de Rosnay, P.,
471 Tavolato, C., Thépaut, J.-N., Vitart, F., 2011. The ERA-Interim reanalysis: configuration and
472 performance of the data assimilation system. *Q. J. Roy. Meteor. Soc.* 137, 553–597.
- 473 Dutra, E., Balsamo, G., Viterbo, P., Miranda, P.M.A., Beljaars, A., Schar, C., E., 2010. An im-
474 proved snow scheme for the ECMWF land surface model: Description and offline validation.
475 *J. Hydrometeorol.* 11, 899–916.
- 476 Frappart, F., Ramillien, G., Leblanc, M., Tweed, S.O., Bonnet, M.P., Maisongrande, P., 2010.
477 Denoising satellite gravity signals by independent component analysis. *IEEE Geosci. Remote*
478 *S.* 7, No. 3, 421–425.
- 479 Frappart, F., Ramillien, G., Leblanc, M., Tweed, S., Bonnet, M.P., Maisongrande, P., 2011. An
480 independent component analysis approach for filtering continental hydrology in the GRACE
481 gravity data. *Remote Sens. Environ.* 115, No. 1, 187–204.
- 482 Hanna, E., Cappelen, J., Fettweis, X., Huybrechts, P., Lickman, A., Ribergaard, M.H., 2005.
483 Observed and modeled Greenland ice sheet snow accumulation, 1958-2003, and links with
484 regional climate forcing. *Hydrol. Process.* 23, 7–30.

- 485 Hanna, E., Cappelen, J., Fettweis, X., Huybrechts, P., Lickman, A., Ribergaard, M.H., 2009.
486 Hydrologic response of the Greenland ice sheet: the role of oceanographic warming. *Hydrol.*
487 *Process.* Vol. 23, p. 7–30.
- 488 Hanna, E., Huybrechts, P., Steffen, K., Cappelen, J., Huff, R., Shuman, C., Irvine-Fynn, T., Wise,
489 S., Griffiths, M., 2008. Increased runoff from melt from the Greenland ice sheet: A response
490 to global warming. *J. Climate* Vol. 21, p. 331–341.
- 491 Howat, I.M., Joughin, I., Fahnestock, M., Smith, B.E., Scambos, T.A., 2008. Synchronous
492 retreat and acceleration of southeast Greenland outlet glaciers 2000–2006: Ice dynamics and
493 coupling to climate. *J. Glaciol.* 54, 646–660.
- 494 Howat, I.M., Joughin, I., Scambos, T.A., 2007. Rapid changes in ice discharge from Greenland
495 outlet glaciers. *Science* Vol. 315, p. 1559–1561.
- 496 Ivins, E. R., James, T. S., 2005. Antarctic glacial isostatic adjustment: a new assessment. *Antarctic.*
497 *Sci.* 17, No. 4, 541–553.
- 498 Jekeli, C., 1981. Alternative methods to smooth the Earth's gravity field. Technical Report.
499 Department of Geodetic Science and Surveying, Ohio State University, Columbus, OH.
- 500 Joughin, I., Howat, I., Alley, R.B., Ekstrom, G., Fahnestock, M., Moon, T., Nettles, M., Truffer,
501 M., Tsai, V.C., 2008. Ice-front variation and tidewater behavior on Helheim and Kangerd-
502 lugssuaq glaciers, Greenland. *J. Geophys. Res.* 113, F01004.
- 503 Krabill, W., Abdalati, W., Frederick, E., Manizade, S., Martin, C., Sonntag, J., Swift, R.,
504 Thomas, R., Wright, W., Yingel, J., 2000. Greenland ice sheet: Height-elevation balance
505 and peripheral thinning. *Science* Vol. 259, No. 5478, p. 428–430.
- 506 Luckman, A., Murray, T., de Lange, R., Hanna, E., 2006. Rapid and synchronous ice-dynamic
507 changes in east Greenland. *Geophys. Res. Lett.* 33, L03503.
- 508 Luthcke, S.B., Zwally, H.J., Abdalati, W., Rowlands, D.D., Ray, R.D., Nerem, R.S., Lemoine,
509 F.G., McCarthy, J.J., Chinn, D.S., 2006. Recent Greenland ice mass loss by drainage system
510 from satellite gravity observations. *Science* Vol. 314, p. 1286–1289.
- 511 Moon, T., Joughin, I., 2008. Changes in ice front position on Greenland's outlet glaciers from
512 1992 to 2007. *J. Geophys. Res.* 113, F02022.

- 513 Mote, T.L., 2007. Greenland surface melt trends 1973-2007: Evidence of a large increase in
514 2007. *Geophys. Res. Lett.* Vol. 34, L22507.
- 515 Murray, T., Scharrer, K., James, T.D., Dye, S.R., Hanna, E., Booth, A.D., Selmes, N., Lickman,
516 A., Hughes, A.L.C., Cook, S., Huybrechts, P., 2010. Ocean regulation hypothesis for glacier
517 dynamics in southeast Greenland and implications for ice sheet mass changes. *J. Geophys.*
518 *Res.* Vol. 115, F03026.
- 519 Paulson, A., Zhong, S., Wahr, J., 2007. Inference of mantle viscosity from GRACE and relative
520 sea level data. *Geophys. J. Int.* 171, 497–5009.
- 521 Peltier, W.R., 2004. Global glacial isostasy and the surface of the ice-age earth: The ICE-5G
522 (VM2) Model and GRACE. *Annu. Rev. Earth Pl. Sc.* 32, 111–149.
- 523 Ramillien, G., Famiglietti, J.S., Wahr, J., 2008. Detection of continental hydrology and glaciol-
524 ogy signals from GRACE: A review. *Surv. Geophys.* Vol. 29, p. 361–374.
- 525 Ramillien, G., Lombard, A., Cazenave, A., Ivins, E.R., Llubed, M., Remy, F., Biancale, R.,
526 2006. Interannual variations of the mass balance of the Antarctica and Greenland ice sheets
527 from GRACE. *Global Planet. Change* Vol. 53, p. 198–208.
- 528 Reynolds, R.W., Smith, T.M., 1994. Improved global sea surface temperature analyses using
529 optimum interpolation. *J. Climate* 7, 929–948.
- 530 Rignot, E., Box, J.E., Burgess, E., Hanna, E., 2008. Mass balance of the Greenland ice sheet
531 from 1958-2007. *Geophys. Res. Lett.* Vol. 35, L20502.
- 532 Rignot, E., Velicogna, I., van den Broeke, M. R., Monaghan, A., Lenaerts, J., 2011. Acceleration
533 of the contribution of the Greenland and Antarctic ice sheets to sea level rise. *Geophys. Res.*
534 *Lett.* 38, L05503.
- 535 Rowlands, D.D., Luthcke, S.B., Klosko, S.M., Lemoine, F.G.R., Chinn, D.S., McCarthy, J.J.,
536 Cox, C.M., Anderson, O.B., 2005. Resolving mass flux at high spatial and temporal resolution
537 using GRACE intersatellite measurements. *Geophys. Res. Lett.* 32, L04310.
- 538 Schmidt, R., Flechtner, F., Meyer, U., Neumayer, K.H., Dahle, Ch., K.R., Kusche, J., 2008.
539 Hydrological signals observed by the GRACE satellites. *Surv. Geophys.* 29, 319–334.

- 540 Sella, Giovanni F., Stein, Seth, Dixon, Timothy H., Craymer, Michael, James, Thomas S., Maz-
541 zotti, Stephane, Dokka, Roy K., 2007. Observation of glacial isostatic adjustment in “stable”
542 North America with GPS. *Geophys. Res. Lett.* 34, L02306.
- 543 Swenson, S., Wahr, J., 2002. Methods for inferring regional surface-mass anomalies from Grav-
544 ity Recovery And Climate Experiment (GRACE) measurements of time-variable gravity. *J.*
545 *Geophys. Res.* 107, No. B9, 2193.
- 546 Tapley, B.D., Bettadpur, S., Watkins, M., Reigber, C., 2004. The Gravity Recovery And Climate
547 Experiment: Mission overview and early results. *Geophys. Res. Lett.* 31, L09607.
- 548 Tedesco, M., Fettweis, X., van den Broeke, M., van de Wal, R.S.W., Smeets, C., van de Berg,
549 W.J., Serreze, M., Box, J.E., 2011. The role of albedo and accumulation in the 2010 melting
550 record in Greenland. *Environ. Res. Lett.* 6, 014005.
- 551 Velicogna, I., Wahr, J., 2005. Greenland mass balance from GRACE. *Geophys. Res. Lett.* Vol.
552 32, L18505.
- 553 Velicogna, I., Wahr, J., 2005. Acceleration of Greenland ice mass loss in spring 2004. *Nature*
554 Vol. 443, 329-331.
- 555 Velicogna, I., 2009. Increasing rates of ice mass loss from the Greenland and Antarctic ice sheets
556 revealed by GRACE. *Geophys. Res. Lett.* Vol. 36, L19503.
- 557 Wahr, J., Molenaar, M., Bryan, F., 1998. Time variability of the earth’s gravity field: Hydrologi-
558 cal and oceanic effects and their possible detection using GRACE. *J. Geophys. Res.* 103, B3,
559 30205–30229.
- 560 Wouters, B., Chambers, D., Schrama, E.J.O., 2008. GRACE observes small-scale mass loss in
561 Greenland. *Geophys. Res. Lett.* Vol. 35, L20501.
- 562 Zwally, H. Jay, Li, Jun, Brenner, Anita C., Beckley, Matthew, Cornejo, Helen G., Dimarzio, John,
563 Giovinetto, Mario B., Neumann, Thomas A., Robbins, John, Saba, Jack L., Yi, Donghui,
564 Wang, Weili, 2011. Greenland ice sheet mass balance: distribution of increased mass loss
565 with climate warming; 2003-07 versus 1992-2002. *J. Glaciol.* Vol. 57, 88-102.

Table 1: Summary of the GRACE-derived mass balance of Greenland

	Data set	Time span	Mass loss [Gt/yr]
Velicogna and Wahr (2005)	CSR (RL01)	04/2004-07/2004	-41±14
Chen et al. (2006)	CSR (RL01)	04/2002-11/2005	-120±6
Velicogna and Wahr (2006)	CSR (RL01)	04/2002-04/2006	-120±6
Luthcke et al. (2006)	mascons	07/2002-07/2005	-101±16
Ramillien et al. (2006)	CNES/GRGS (RL01)	07/2003-03/2005	-109±9
Wouters et al. (2008)	CSR (RL04)	02/2003-01/2008	-179±25
Baur et al. (2009)	CSR (RL04)	08/2002-07/2008	-222±13
	GFZ (RL04)	08/2002-07/2008	-178±22
	JPL	08/2002-07/2008	-88±21
Velicogna (2009)	CSR (RL04)	04/2002-02/2009	-230±33
Chen et al. (2011)	CSR (RL04)	04/2002-11/2009	-219±38
this study	CSR (ICA-400km+STL)	04/2002-07/2010	-66±1
	CSR (GAUSS-400km + STL)	04/2002-07/2010	-92±1
	GFZ (ICA-400km + STL)	04/2002-07/2010	-63±1
	GFZ (GAUSS-400km + STL)	04/2002-07/2010	-81±1
	JPL (ICA-400km + STL)	04/2002-07/2010	-51±1
	JPL (GAUSS-400km + STL)	04/2002-07/2010	-32±1

567 7. Figure Captions

568 Figure 1: Geographical map of the Greenland Ice Sheet (GrIS) which is portioned into 6
569 mean ice fields according to Luthcke et al. (2006) (a), and the locations of continental (G) and
570 on-sea (S) points used in this study for signals comparison (b).

571

572 Figure 2: Time series of water-equivalent mass of GrIS derived from GRACE solutions of dif-
573 ferent providers (CSR - blue; GFZ - red; JPL - green), and using different types of filtering
574 (Gaussian with a radius of 400 km + ICA - plain lines; Gaussian with a radius of 400 km - dot-
575 ted lines) (top), and the corresponding interannual time series after STL decomposition (bottom).

576

577 Figure 3: Histograms of trend estimates using different providers (CSR, GFZ, JPL) and vari-
578 ous time spans, considering a simple linear adjustment after no STL decomposition (a), and after
579 STL decomposition (b). Error bars are from analysis of normal equation for a posterior standard
580 deviation on the adjusted linear slope from observation uncertainties. These latter uncertainties
581 were obtained from formal errors on the monthly Stokes coefficients.

582

583 Figure 4: Geographical maps of mass trends over the GrIS using GFZ solutions post-processed
584 using Gaussian filtering with a radius of 400 km + ICA, and corrected from PGR using the Paul-
585 son's tuning of the model ICE-5G, over the period 02/2003-12/2007 with no STL decomposition
586 (a), and with STL decomposition (b), and over the period 02/2003-07/2010 with no STL decom-
587 position (c) and with STL decomposition (d).

588

589 Figure 5: Interannual mass change time series obtained after STL decomposition from CSR,
590 GFZ, and JPL GRACE solutions for the six mean ice fields (see Fig. 1), and considering differ-
591 ent types of post-processing (low-pass Gaussian filtering with a radius of 400 km + ICA - plain
592 lines; Gaussian filtering with a radius of 400 km - dotted lines).

593

594 Figure 6: Correlation GrIS maps between interannual STL-decomposed time series of GRACE-
595 based mass variations and snow depth changes from ECMWF reanalysis: a) CSR (ICA 400 km),
596 b) CSR (Gaussian 400 km), c) GFZ (Gaussian 400 km), d) JPL (Gaussian 400 km).

597

598 Figure 7: Interannual trends after STL decomposition of the GRACE-based mass time series
599 (CSR, GFZ, JPL) and snow depth from ECMWF reanalysis and considering different types of

600 post-processing (low-pass Gaussian filtering with a radius of 400 km + ICA - plain lines; Gaus-
601 sian filtering with a radius of 400 km - dotted lines) for the six ice fields.

602

603 Figure 8: Local comparisons between time series of GRACE-based GrIS mass change and Sea
604 Surface Temperature (SST) from NOAA for different couple of points (see Fig. 1 for the loca-
605 tions of these points).

606 **8. Figures**

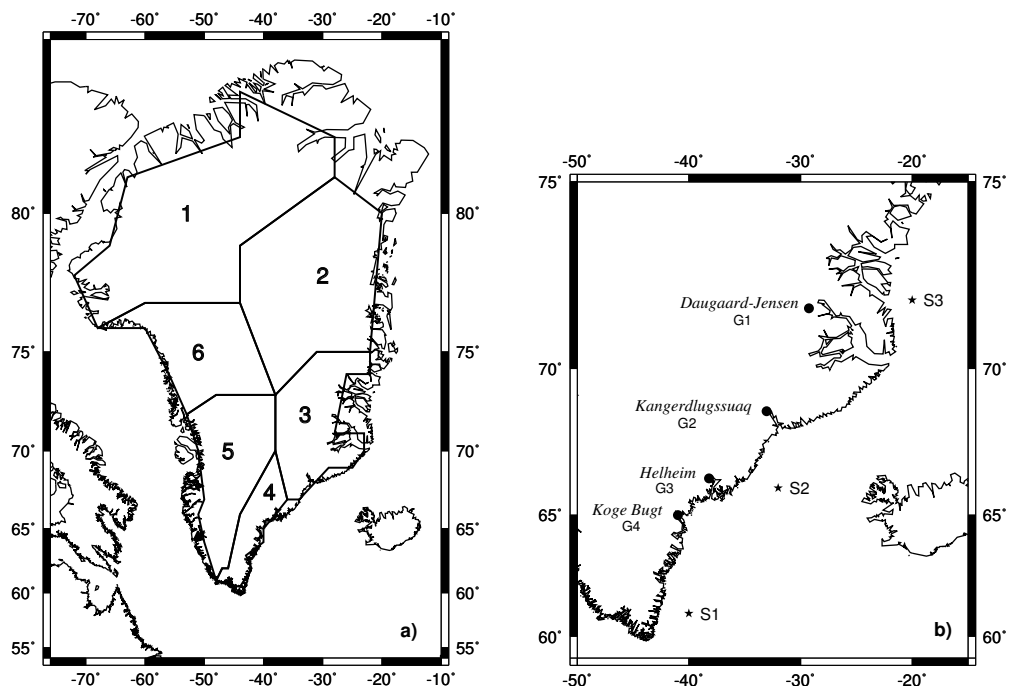


Figure 1

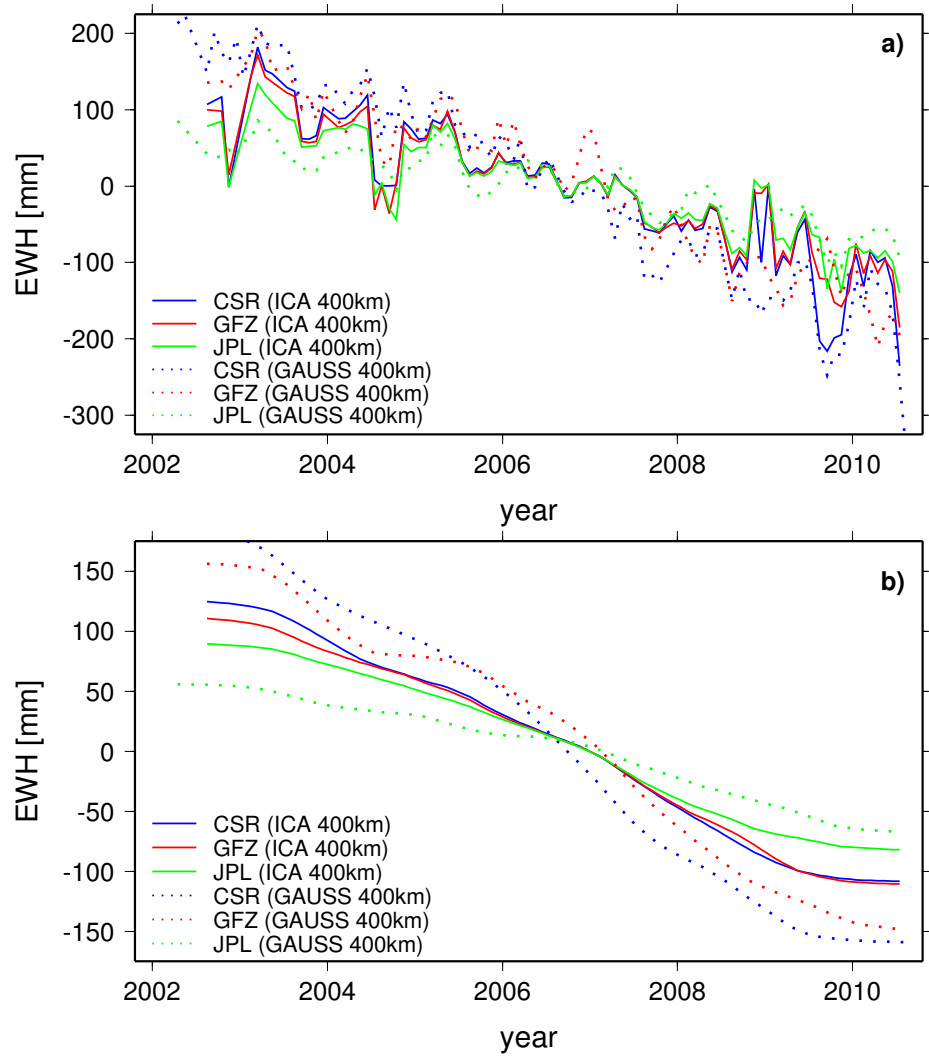


Figure 2

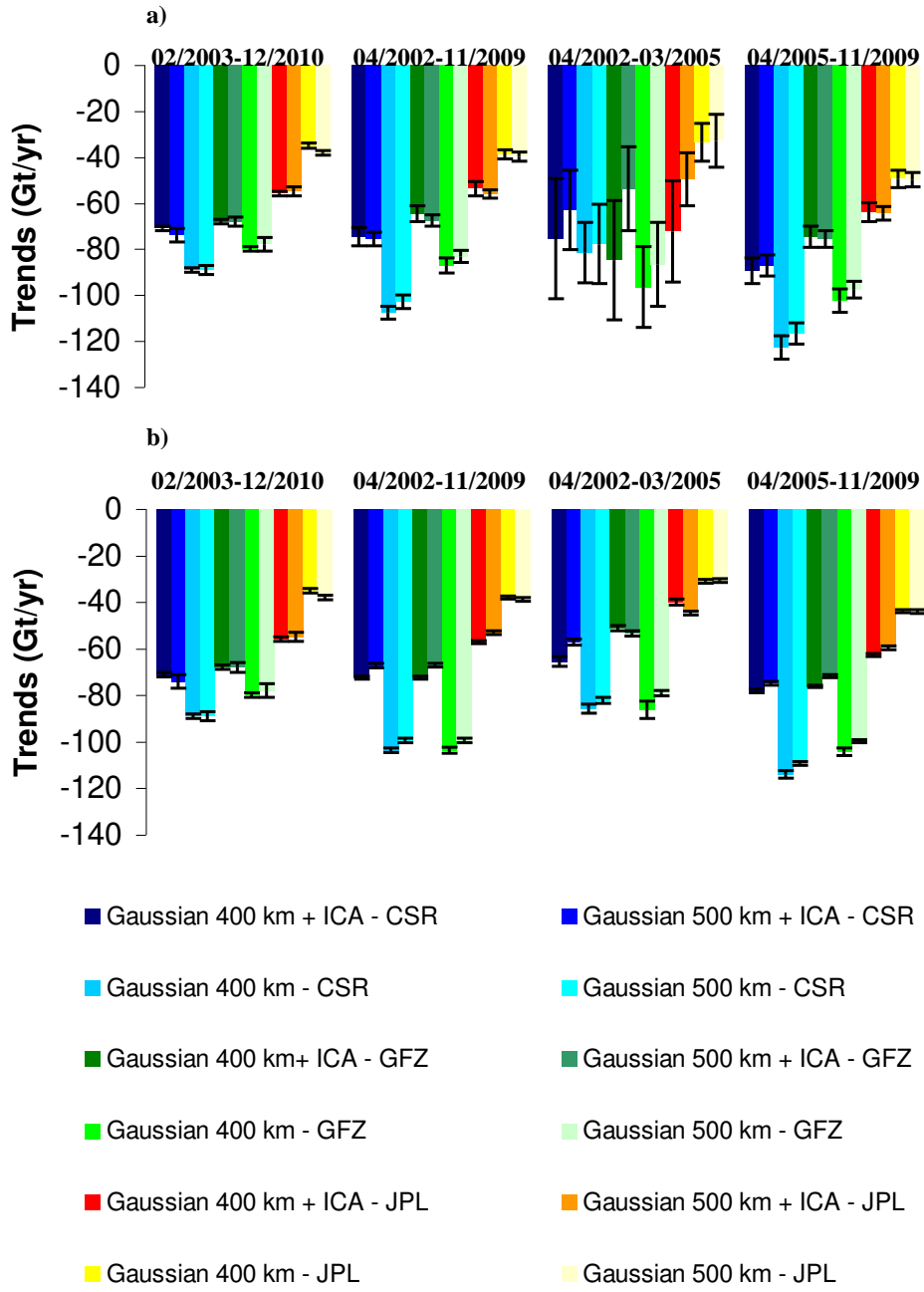


Figure 3

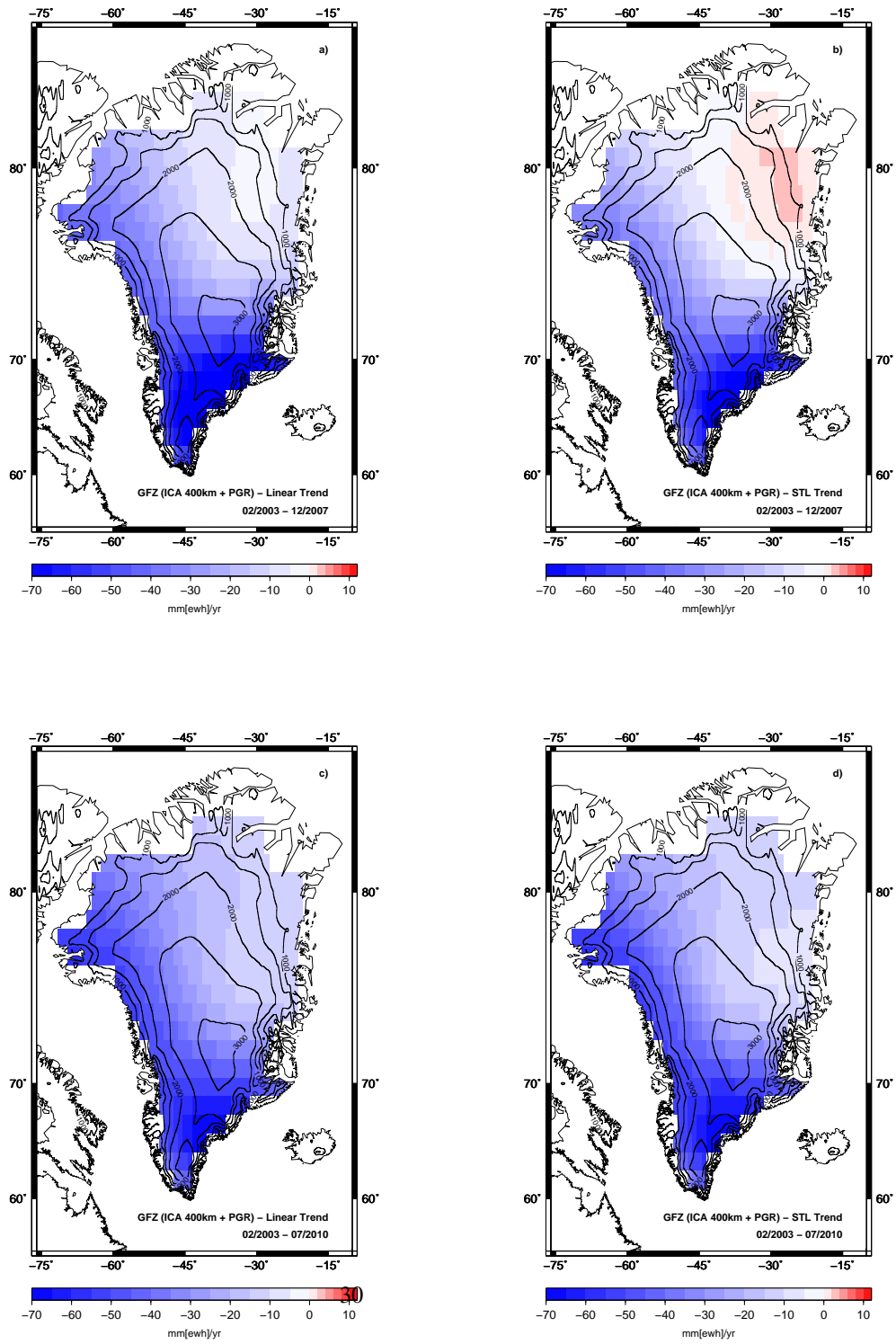


Figure 4

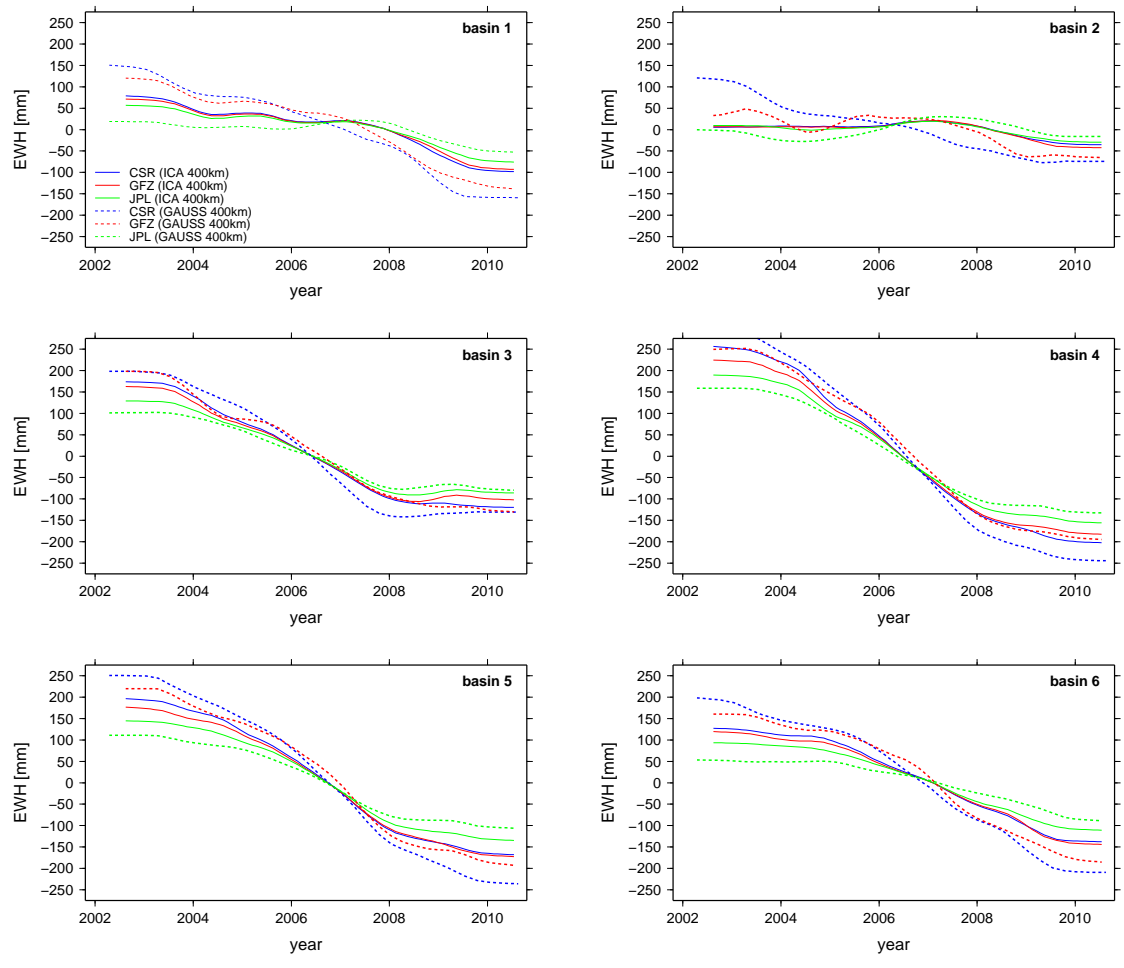
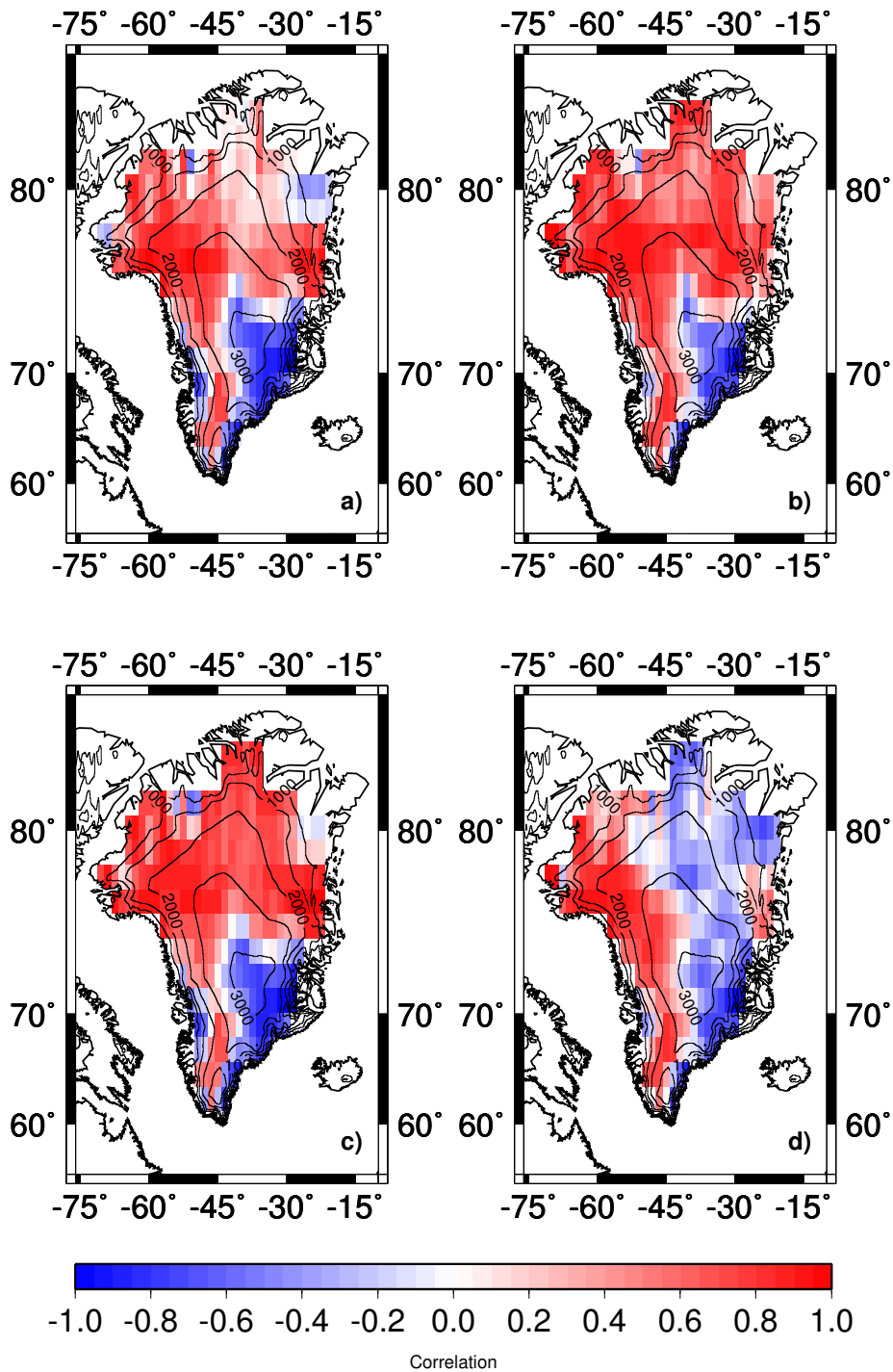


Figure 5



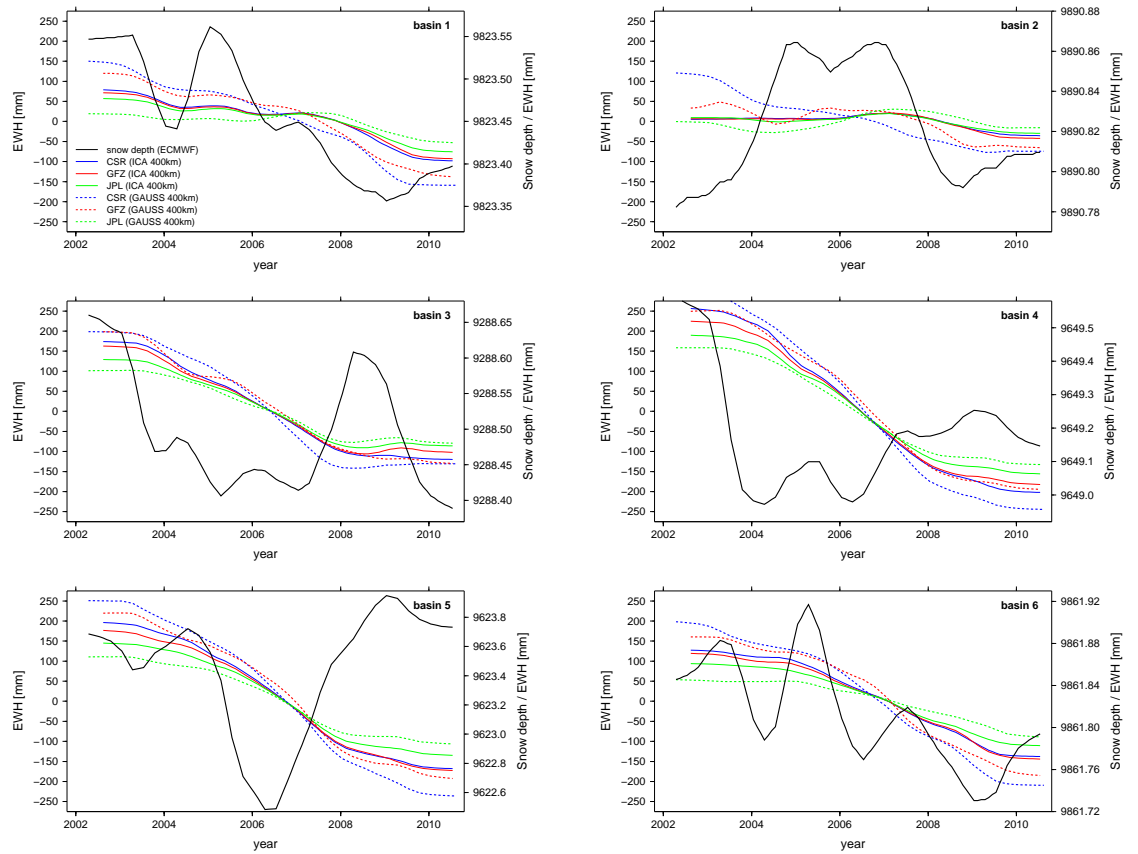


Figure 7

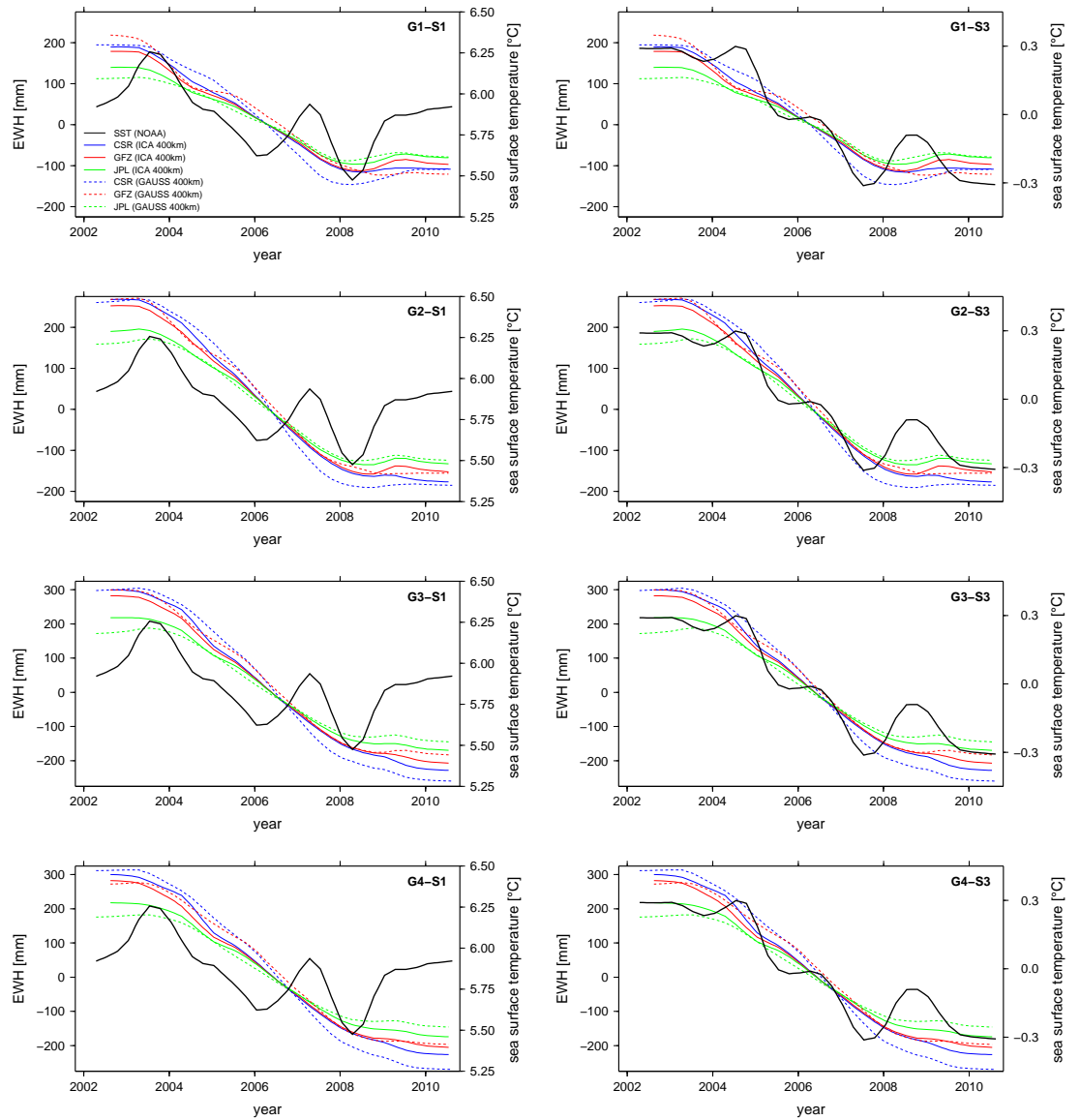


Figure 8